*Express Polymer Letters Vol.17, No.2 (2023) 196–210*
*Available online at www.expresspolymlett.com*
*https://doi.org/10.3144/expresspolymlett.2023.14*

*Research article*

# Valorization of nylon and viscose-rayon textile yarn wastes for fabricating nanocomposite films

*Prince Kumar Mishra, Arihant Ahuja, Bhupender Kumar Mahur, Vibhore Kumar Rastogi*[*]*

Department of Paper Technology, Indian Institute of Technology Roorkee, 247667 Uttarakhand, India

*Received; 7 July 2022 accepted in revised form 19 September 2022*

---

**Abstract.** In this work, two types of pre-consumer textile waste, namely, viscose-rayon and nylon yarn, were utilized for nanocomposite filmmaking using the green solvent casting method. The nanocellulose was extracted from the viscose-rayon and incorporated as a filler in nylon films. The effects of nanocellulose on thermal, chemical, mechanical, structural, and barrier properties of films containing 0.1, 0.5, and 1 wt% nanocellulose were investigated in detail. The thermal study of films using differential scanning calorimetry (DSC) confirmed that adding nanocellulose into the nylon matrix does not act as a nucleating agent as nylon yarn waste already had ~5 wt% nucleating agents (thermogravimetric analysis, TGA). Rather, a decrease in the crystallinity of films was determined with the addition of nanocellulose. No significant changes in the mechanical properties were observed for nylon nanocomposite films. However, an increased hydrogen bonding was observed between the nanocellulose and nylon, along with the reorientation of hydrogen bonds (Fourier-transform infrared spectroscopy, FTIR). A dense cross-section and structured surface were observed in the scanning electronmicroscopic (SEM) images for nanocomposite films. The water vapor barrier of films increased as the concentration of nanocellulose increased in the nylon films and resulted in a 55% decrease in water vapor transmission rate (WVTR) compared to neat nylon film.

***Keywords:*** *nanocomposites, nylon yarn textile waste, viscose-rayon yarn waste, nanocellulose, waste valorization*

---

## 1. Introduction

The textile industry generates a large amount of waste, leading to waste accumulation, greenhouse gas emissions, and environmental pollution. Textile wastes are often classified as pre-consumer (fibers, yarns, fabrics, and mixed fiber/yarn/fabric with chemicals), post-consumer (discarded garments), and industrial waste (technical textiles, carpets, durries, conveyor belts, industrial ropes, drive belts, medical textiles). Most of these discarded textiles can be recycled but are landfilled or incinerated due to the cost involved [1]. Textile waste can be valorized depending on its type, form, and usability. A recent review on the valorization potential of textile wastes is presented elsewhere [2]. Textile wastes could be valorized for numerous applications, including textile manufacturing, energy generation [3], building materials [4], packaging film [5], paper [6], and composites [7]. Textile waste includes fiber/yarn/fabric of cotton, cellulose (viscose, flax, hemp, kapok, rami), wool, polyester (PET), nylon-6, acrylic, and polypropylene.

Recently, viscose-rayon has been gaining much attention as a raw material for green textiles [8]. It is a manmade regenerated cellulosic textile produced from the wet spinning process of natural sources like woods [9, 10] that are later converted into yarns. Yarns are further used in textile weaving, hand-knotted carpet weaving, home furnishing, and industrial textile applications [9, 10]. In the textile weaving processes, a huge amount of cut viscose-rayon yarns waste is generated [11, 12], which is either incinerated or landfilled [1, 13]. A few research articles have been reported on the valorization potential of

---

[*]Corresponding author, e-mail: vibhore.rastogi@pt.iitr.ac.in

viscose-rayon for energy production [14], reinforcement in building materials [4], reinforcement in polymer composite [15], and extraction of nanocellulose (NC) [16]. Viscose-rayon consists of pure alpha-cellulose and hence possesses numerous surface hydroxyl groups, which are reactive and interact strongly with the polar polymer matrix; otherwise, the presence of lignin and hemicellulose as in native cellulose fibers resulted in weak interactions with a polar matrix like nylon [20].

Nylon-6 is a synthetic polymer extensively used in textile production [17], packaging [18], composites [19], and many other applications [3, 20–23] due to its excellent mechanical and thermal properties, transparency, and resistance to chemicals [24]. Consequently, an enormous amount of nylon waste is generated annually, which needs urgent attention. Packaging and composite waste of nylon often contain multi-layered components [25], which makes recycling or valorization cumbersome. However, a few research articles on nylon textile waste valorization are reported for applications like insulation material [21], building material [20], energy [23], and filtration membrane [22] due to the simplicity and purity of nylon-6 in textile waste. The industrial-grade of nylon-6 is often reinforced with cellulosic-based fibers like flax, hemp, hardwood [19], nano/microfibrillated cellulose (NFC/MFC) [26], and cellulose nanocrystals (CNC) [27] to enhance the mechanical properties of composites. The tensile strength increased by 23.82% with the addition of fibers, and lower crystallinity was observed with the addition of NFC/MFC and CNC. Apart from cellulosic fillers, graphene has been previously added to the recycled nylon-6 matrix to enhance the tensile strength of the films at a lower concentration of 2 wt% [28]. In another study impact strength of recycled nylon-6 was improved by 55.5% with the addition of Hytrel (elastomer) [29]. However, for packaging applications, both mechanical and barrier properties (like oxygen transmission rate, OTR, and water vapor transmission rate, WVTR) of pure nylon-6 were targeted by blending with nanoclays like montmorillonite [30] and Cloisite 30B [31], which increased oxygen barrier by 2.8 times. With the continuous trend of sustainability, green fillers are favored. In addition, waste management practices leading to waste-to-wealth and circular economy are the prime concern of many counties [32]. Nylon-6 is used as a packaging material where an oxygen barrier is required, but it absorbs water and loses its barrier properties because it is hygroscopic. Therefore, it is a sandwiched layer for packaging applications [18]. Inorganic materials such as nanoclay have enhanced water and oxygen barrier properties of nylon-6 [30]. The barrier properties of nylon-6 textile waste can also be enhanced using bio-based nanomaterials like nanocellulose, but it is never reported and explored. Due to the presence of polar groups in nylon-6, it is expected to have higher compatibility with the hydroxyl groups of cellulose [20], along with good dispersion. Thus, compatibilizers or coupling reagents are not needed for composites.

In the present study, powdered nanocellulose was incorporated (derived from viscose-rayon textile waste) in the nylon-6 matrix (obtained from nylon textile yarn waste) to produce nanocomposite films. A detailed raw material analysis of nylon textile waste was conducted, revealing a few nucleating agents, plasticizers, and antioxidants in nylon textile yarn waste. Nanocomposite films containing a variable amount of nanocellulose were characterized for their morphological (field emission scanning electronmicroscopy, FESEM; atomic force microscopy AFM), chemical (FTIR), thermal (TGA, DSC), mechanical (universal testing machine, UTM), and barrier properties (WVTR, contact angle). This work emphasized the importance of nanocellulose extraction from viscose yarn waste and used it as a green filler for the nylon matrix. In addition, nylon yarn textile waste was proposed as a cheap alternative to expensive industrial-grade nylon-6 for various appropriate applications.

## 2. Materials and methods

### 2.1. Materials

Nylon scrap yarn waste was collected from Kusumgar Corporates Pvt. Ltd. (Textile Mill, Vapi, Gujrat, India), and the viscose-rayon yarn waste was obtained from a local yarn vendor (Bhadohi, Uttar Pradesh, India). Sulphuric acid (97% pure) and acetic acid (98% pure) were purchased from Avantor Performance Materials India Limited (India).

### 2.2. Sample preparation

### 2.2.1. Extraction of nanocellulose from viscose-rayon yarn waste

The acid hydrolysis technique was adopted from elsewhere [16] to extract nanocellulose from viscose yarn waste. First, the viscose yarn was cut into small fibers, washed thoroughly with hot water, and dried. The 64 wt% $H_2SO_4$ solution was prepared and cooled in an ice bath. 1 g of viscose yarn was slowly added to 20 ml of cold 64 wt% $H_2SO_4$ solution under stirring to avoid the decomposition of viscose yarn. Further, heating was done at 40 °C in an oil bath placed over a hot plate magnetic stirrer. The hydrolyzed sample was collected after the reaction time of 30 minutes and appeared white, suggesting no over degradation of nanocellulose, which would otherwise turn dark yellowish [16]. The suspension was immediately cooled by adding 400 ml of cold deionized water to stop the reaction, and the pH was also increased from 1 to 3. A turbid supernatant of nanocellulose suspension was formed and kept for settling down for over 48 hours that was later drained and collected. To eliminate the free excess acid from the nanocellulose, a semi-permeable membrane was used for dialysis against deionized water for 72 hours until a neutral pH was attained. Finally, the nanocellulose sample was ultrasonicated, refrigerated at –40 °C, and further lyophilized at –70 °C to obtain nanocellulose powder.

### 2.2.2. Fabrication of neat nylon and nylon nanocomposite films

Nylon yarn waste was washed thoroughly with hot water to remove any surface impurities and later dried and stored at 23 °C and 50% *RH*. Neat nylon and nanocomposite films were developed using acetic acid as a green solvent by the solution casting method. 0.4 g of nylon yarn was dissolved in 27 ml of acetic acid (1.5% w/v). The stirring was done for 45 minutes at 80 °C using a temperature-controlled hot plate magnetic stirrer. The nanocellulose powder derived from viscose yarn waste was dispersed into nylon acetic acid solution under continuous stirring for 5 minutes with a concentration of 0% (neat, control), 0.1, 0.5, 1, and 2 wt%. The resulting solution was then cast into 90 mm diameter glass Petri dishes using a surface leveler to obtain films of uniform thickness. The solvent was evaporated in a hot air oven at 50±3 °C for 12 hours, and films were peeled off from the Petri dishes. Before physical, chemical, and mechanical testing, the prepared nylon nanocomposite films were stored at 23 °C and 50% *RH* in a regulated environment [33]. All prepared films will be denoted as Neat Nylon (nylon film with 0% nanocellulose), Nylon-0.1% (nylon film with 0.1% nanocellulose), Nylon-0.5% (nylon film with 0.5% nanocellulose), Nylon-1% (nylon film with 1% nanocellulose), and Nylon-2% (nylon film with 2% nanocellulose) throughout the text.

## 2.3. Characterization

### 2.3.1. Fourier transform infrared spectroscopy (FTIR)

Attenuated total reflection Fourier-transform infrared spectroscopy or ATR-FTIR was conducted to determine the chemical composition of nylon yarn waste, viscose yarn waste, nanocellulose, and nanocomposite films, using Perkin Elmer, C91158 spectrophotometer (Chicago, USA). FTIR spectra were collected between 4000 and 500 $cm^{-1}$ wavenumbers with a resolution of 4 $cm^{-1}$ and averaged over 16 scans. The spectra were baseline corrected and normalized for comparative analysis to determine the changes in chemical content.

### 2.3.2. Field emission-scanning electron microscopy (FESEM)

The variation in surface and cross-section morphologies of nylon yarn waste, viscose yarn waste, nanocellulose, and nanocomposite films was inspected by Field Emission Scanning Electron Microscopy (MIRA3 LMH Tescan, USA), operating at an accelerating voltage of 5 kV. The cross-sections were obtained by cryo-fracturing in liquid nitrogen. Each sample was sputter-coated with a thin gold layer (2–10 nm) using glow discharge plasma to improve conductivity and picture clarity [34].

### 2.3.3. Atomic force microscopy (AFM)

The nanoscale's topography of nanocellulose produced from viscose waste was further studied with atomic force microscopy (AFM, Bruker Dimension Icon AFM, USA). A dilute suspension of nanocellulose was probe sonicated and drop cast over a glass slide. The glass slide was dried overnight at ambient conditions, and images were obtained in Scan Assist mode using silicon nitride tips. The diameters of nanocellulose were analyzed using Nanoscope analysis software.

### 2.3.4. Differential scanning calorimetry (DSC)

The thermal behavior of nylon yarn waste and all fabricated nylon-based nanocomposite films was studied using differential scanning calorimetry (TA Instruments, New Castle, DE, USA, DSC 25) under a constant nitrogen gas flow. Double heating cycles with an intermediate cooling cycle were performed on each 5 mg weight sample (sealed in aluminum pans). To erase the thermal history, samples were heated from 0 to 250 °C at 10 °C/min during the first heating cycle and maintained at 250 °C for 2 minutes before being cooled to 0 °C at 10 °C/min. The sample was then heated a second time at 10 °C/min from 0 to 250 °C. Three measurements were taken for each sample. The thermogram's second heating cycle was used to determine the glass transition ($T_g$), melting point ($T_m$), and melting enthalpy ($H_m$). The cooling cycle was used to measure the temperature of melt crystallization ($T_{mc}$). Equation (1) was used to calculate the total crystallinity ($X_c$) of nylon yarn waste and nylon-based nanocomposite:

$$X_c = \frac{\Delta H_m}{\Delta H_m^0 (1-\alpha)} \cdot 100 \tag{1}$$

where the melting enthalpy of the generated crystals in the nylon-6 is $\Delta H_m$, while the theoretical enthalpy value for a 100% crystalline nylon-6 is $\Delta H_m^0$ (190 J/g) [35], and α is the weight fraction of nanocellulose content in nanocomposite films.

### 2.3.5. Thermogravimetry analysis (TGA)

The thermal degradation behavior of samples was studied using thermogravimetric (TA Instruments, New Castle, DE, USA, TGA 55). The sample weight of around 5 mg was heated from 25 to 600 °C at 10 °C/min (ASTM E1131). The testing was conducted in a nitrogen gas atmosphere with a 20 ml/min gas flow rate.

### 2.3.6. Thickness and mechanical properties of films

A digital micrometer (Lorentzen & Wettres, Stockholm, Sweden) was used to measure the thickness of the neat nylon and nanocomposite films. Each sample was measured at five different locations and reported as a mean with a standard deviation.

Mechanical properties such as tensile strength and percentage elongation at break were determined using the Universal Testing Machine (INSTRON 3365, Integrated System Solutions, Bengaluru, India). Rectangular strips of dimension 10×40 mm$^2$ were cut by a cutting die and tested with a primary grip separation of 20 mm at a 1 mm/min crosshead speed. Each sample was replicated three times.

### 2.3.7. Water contact angle and water vapor transmission rate (WVTR) of films

The surface wettability of films was measured by the sessile drop test method using a contact angle analyzer (DSA25 KRÜSS GmbH, Germany). A droplet volume of 5 µl was placed on films using a microsyringe. The measurements were repeated three times per sample.

As described in ASTM E96/E96M-16, the desiccant method was used to calculate the WVTR of all samples. Around 10 g of dried silica gel was placed in glass vials with an opening mouth area of 2.27 cm$^2$. The developed films were securely sealed on top of the glass vials. The glass vials were then placed in a desiccator with a saturated sodium chloride solution to maintain a relative humidity of 75%. The desiccators were then sealed with paraffin wax and kept in a 25 °C oven. The weights of the cups were taken at the start and every 24 hours for a total of 10 days. Each sample was replicated three times. The slope [g/day] of the curve drawn between weight and days, divided by transfer area, *i.e.*, 2.27 cm$^2$, was used to calculate WVTR [g/(m$^2$·day)].

## 2.4. Statistical analysis

With the help of statistical software SPSS ver. 26, the experimental data were statistically analyzed to estimate the analysis of variance (IBM Corporation, Armonk, USA). The Tukey *post hoc* test ($p < 0.05$) was used to see if there were any significant changes. Small alphabets in superscripts were assigned next to the values. Different letters in the respective column indicate a significant difference in values considering a 95% confidence level.

# 3. Results and discussion

## 3.1. The threshold concentration of nanocellulose in nylon films

The nylon films with varying concentrations of nanocellulose were prepared and placed over the printed white logo on black paper, presented in Figure 1. All films appeared to be transparent, smooth, and without cracks. As the concentration of nanocellulose increased, the films became slightly cloudier. At 2 wt% nanocellulose, the film appeared white, brittle, and developed cracks. The brittle nature of the film might be due to increased bonding between the hydroxyl groups of nanocellulose and amine group of nylon, leading to arresting of nylon's crystallization

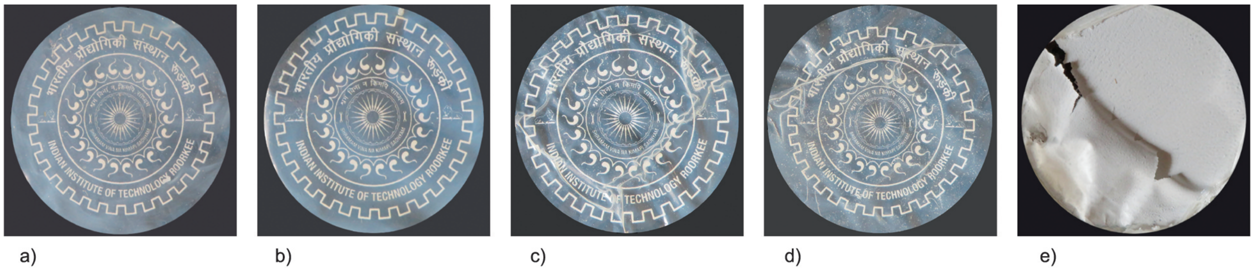

**Figure 1.** Photographs of solvent cast nylon-nanocellulose films showing (a) neat Nylon film, (b) Nylon-0.1% film, (c) Nylon-0.5% film, (d) Nylon-1% film, and (e) Nylon-2% film.

into the amorphous form and thus resulting in disrupted internal bonding between the nylon polymeric chains leading to cracks [36]. Therefore, nanocellulose up to 1 wt% was selected as a threshold concentration of filler in nylon films, and Nylon-2% was not characterized further.

### 3.2. The thickness of the films

The thickness plays a crucial role in a polymer's physical and functional properties. Table 1 indicates the thickness of the nanocomposite films. It can be observed that all films were uniform and varied in thickness in the range of 48–53 µm. No significant differences in thickness were determined for all films. The thickness of the films was also aligned with the thickness observed in the FESEM images performed on the cross-section of the films (will be shown later).

**Table 1.** The thickness of neat nylon and nylon nanocomposite films.

| Sample | Thickness [µm] |
|---|---|
| Neat nylon | 48±2.74$^a$ |
| Nylon-0.1% | 54±5.48$^a$ |
| Nylon-0.5% | 49±4.18$^a$ |
| Nylon-1% | 53±2.71$^a$ |

The mean and standard deviation are used to express the data. $^a$Different letters in the same column indicate significant differences ($p < 0.05$). (There are no significant diffences.)

### 3.3. Fourier transform infrared spectroscopy

FTIR was used to analyze raw fiber waste, fabricated nanocellulose, and nanocomposite films. Figure 2a shows the absorption bands for viscose-rayon yarn waste and extracted nanocellulose; a broad peak around 3400 cm$^{-1}$ (–OH stretching), 2920 cm$^{-1}$(CH$_2$ symmetrical and asymmetrical stretching), 1642 cm$^{-1}$ (C=O stretching), 1432 cm$^{-1}$ (CH$_2$ symmetric bending), 1372 cm$^{-1}$ (C–H bending), 1150 cm$^{-1}$ (C–O–C asymmetric stretching), 1020 cm$^{-1}$ (C–O stretching), 895 cm$^{-1}$ (C–O–C stretching) and 670 cm$^{-1}$ (C–H bending), as described previously [16, 37–43]. Similarly, the characteristics peaks of nylon yarn waste (Figure 3a) shows a broad peak around 3400 cm$^{-1}$ (–OH stretching), 3291 cm$^{-1}$ (N–H stretching bond), 2925 cm$^{-1}$ (CH$_2$ asymmetric stretching), 2853 cm$^{-1}$

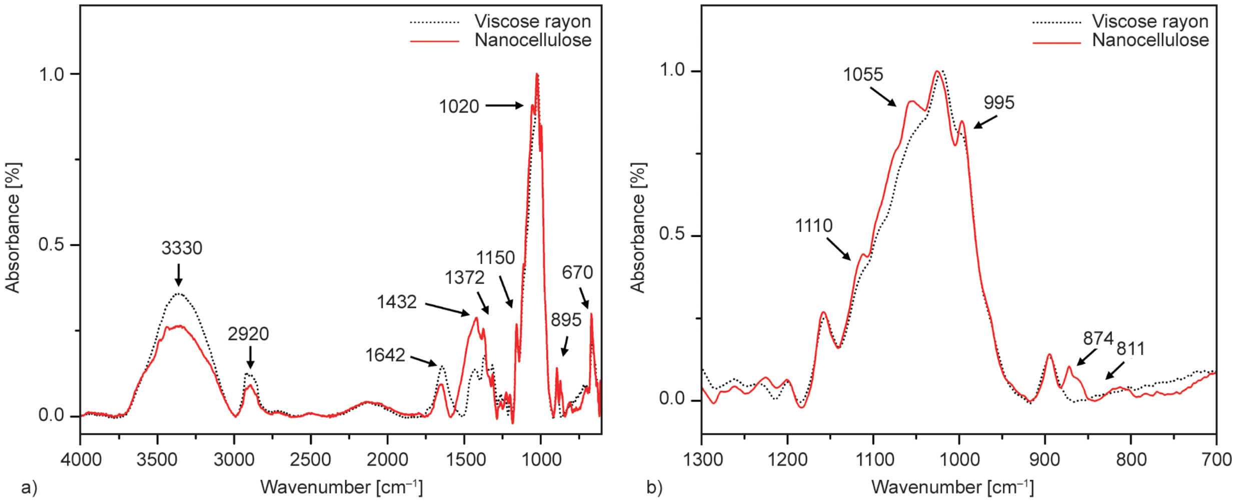

**Figure 2.** FTIR plots of viscose yarn and nanocellulose in the wavenumber of (a) 4000 to 600 cm$^{-1}$ and (b) magnified at 1300 to 700 cm$^{-1}$.

(C–H stretching), 1633 cm$^{-1}$ (C=O (amide-I) stretching), 1534 cm$^{-1}$ (N–H (amide-II) deformation), 1367 cm$^{-1}$ ($CH_2$ wagging), and 1261 cm$^{-1}$ ($CH_3$ bending), 1025 cm$^{-1}$ (C–O stretching) and 695 cm$^{-1}$ (C–H bending), as reported in previous literature [44]. From Figure 2a, the appearance of new peaks at 874 and 811 cm$^{-1}$ was only observed in the nanocellulose sample representing C–O–$SO_3$ group vibration, attributed to the presence of sulfonate esters on the nanocellulose surface during sulphuric acid hydrolysis [45, 46]. Several other bands related to sulfonate esters were also reported in the literature ranging from 1350 to 750 cm$^{-1}$ [45]. Due to the increase in the surface area of nanocellulose compared to viscose, it was expected that the peak intensity around 3330 cm$^{-1}$ should be higher for nanocellulose because of more free hydroxyls (–OH) at the surface. Rather a decrease in the 3330 cm$^{-1}$ peak was visible in the nanocellulose sample. A similar observation was noted qualitatively in the case of nanocellulose extracted using sulphuric acid [16]. This decrease in peak intensity results from converting a few surface hydroxyls of nanocellulose with sulfonyl groups, thereby reducing the overall hydroxyls present on the surface. Moreover, the intensity of several nanocellulose peaks (1432 and 1371 cm$^{-1}$) was higher than viscose. The higher peak at 1110, 1055, and 995 cm$^{-1}$ might be due to higher C–O–C ether linkages that were developed after acid hydrolysis and thereby resulted in an increased crystallinity of nanocellulose [47] (Figure 2b). The spectra were normalized on cellulose ring-related bands (1200 to 850 cm$^{-1}$).

The crystallinity index was calculated for viscose-rayon and nanocellulose from the peak intensity ratio of 1373/2900 cm$^{-1}$ [48]. The crystallinity index for viscose and nanocellulose was 1.48 and 2.82, respectively. The increased crystallinity of nanocellulose compared to viscose fiber is in line with the previous studies [16], as sulphuric acid degrades the amorphous part of cellulose and thus increases the crystallinity of cellulose.

To compare the chemical composition of nylon yarn waste and nylon films, the spectra were normalized at 1168 cm$^{-1}$ [49, 50]. From Figure 3a, a broad peak around 3460 cm$^{-1}$ (–OH stretching) was observed in nylon yarn waste, which is usually absent or very weak in the spectrum of industrial-grade nylon pellets [51]. It indicates the presence of additives like talc powder (as a nucleating agent) or phenols (antioxidant) in the nylon yarn that is usually added to enhance the mechanical properties and thermal stability, respectively, during the manufacturing process of nylon fibers for textile application [52]. The presence of phenols in nylon yarn waste was further confirmed by a peak at 750 cm$^{-1}$. Hot water washing of nylon yarn before film formation might remove the extra talc on the surface of the yarn and lead to a reduction in the peak of 3400 cm$^{-1}$ in the neat nylon film. Similarly, solvent processing of nylon yarn at 80 °C completely oxidized the antioxidant present, and hence peak at 750 cm$^{-1}$ was absent in films. Peaks at 17201 and 1740 cm$^{-1}$ (C=O stretching) in nylon yarn indicated the presence of plasticizers that are often added to nylon during the processing of nylon yarn to avoid runnability issues and to provide elasticity to yarn [17]. It is also observed that peak intensity at 3300 cm$^{-1}$ (hydrogen-bonded N–H stretching) increased for neat nylon film compared to nylon

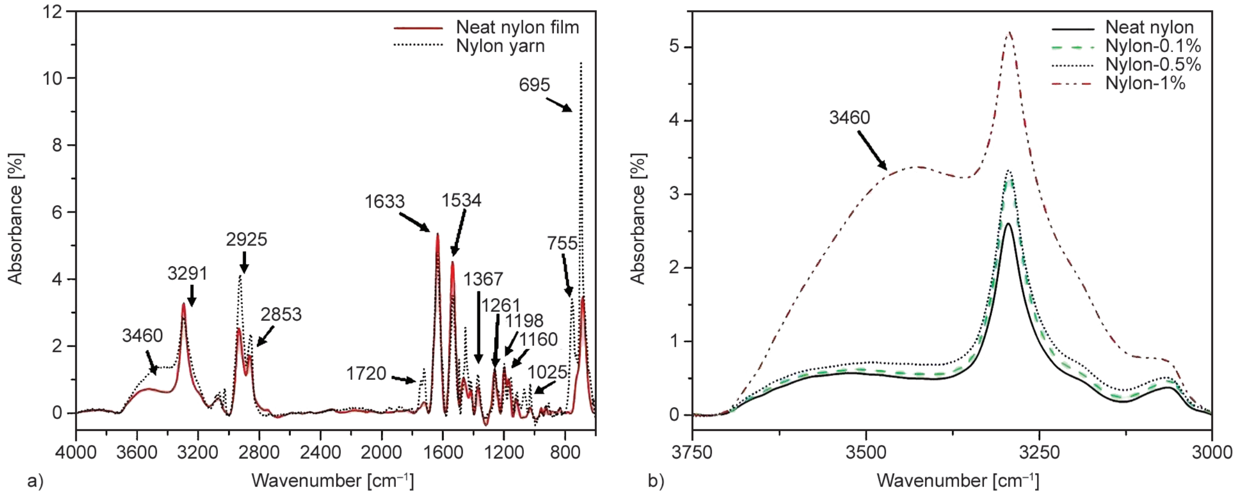

**Figure 3.** FTIR spectra of (a) nylon yarn and neat nylon film and (b) neat nylon and nylon nanocomposite films containing nanocellulose.

yarn, which is attributed to solvent processing providing easy mobility to polymeric chains leading to new hydrogen bond formation. In contrast, a reduction in the peak intensity at 695, 1198, 1367, 1418, 2925, and 2850 cm$^{-1}$ for neat nylon film was evident compared to the nylon yarn waste. This observation is attributed to the conversion of α-crystalline form (stable) of nylon to γ-crystalline form (metastable) that was mediated through solvent processing [51].

As the concentration of nanocellulose in the films was very low (≤1%) and the limitations of FTIR to sense the material up to a few microns deep inside the film [53], the prominent characteristic peak of nanocellulose (1200 to 900 cm$^{-1}$) was not visible in the nanocomposite films (data not shown). From Figure 3b, with the addition of nanocellulose in the nylon films, a continuous increase of broad peak at 3460 cm$^{-1}$ was observed, attributed to the formation of new hydrogen bonds with the OH groups of cellulose and amide groups of nylon [51]. At the maximum concentration of nanocellulose in the film (1%), the peak intensity at 3460 cm$^{-1}$ increased abruptly, possibly due to the increased hydrogen bonding between the nanocellulose and the nylon that reoriented the original hydrogen bonding in the nylon polymeric chain [51].

### 3.4. Field emissions-scanning electron microscopy

FESEM was used to analyze the surface morphology and cross-section of fiber waste, nanocellulose, and prepared nylon nanocomposite films. Figure 4a and Figure 4c illustrate the surface of the viscose and nylon yarn waste (as received), respectively. From the surface of viscose yarn, fine longitudinal lines or striations of a single viscose fiber are visible. The flower-like surface of viscose fiber is due to the shape of the spinneret used in the wet spinning of viscose fibers. In contrast, the nylon yarn waste showed a uniform rod-like surface appearance with few impurities at the surface that might be talc powder (Figure 4d), which were absent from the viscose yarn (Figure 4b). The diameter from FESEM images was observed as 35.71±9.42 µm for nylon yarn and 11.47±4.01 µm for viscose-rayon yarn.

Nanocellulose was extracted using viscose-rayon yarn waste by acid hydrolysis. The FESEM of nanocellulose was performed by drop-casting the nanocellulose water suspension onto the glass plate. The nanocellulose appeared as small aggregates (Figure 5a) with irregular shapes (Figure 5b). The irregular shapes of nanocellulose were due to strong swelling treatments by NaOH in the wet spinning process of viscose-rayon fiber from wood and had already been reported in past research [16]. At higher magnification, nanocellulose aggregates' diameter appeared to be less than 100 nm (Figure 5b).

The FESEM images of all the nylon films are shown in Figure 6. The surface image of the neat nylon film (Figure 6a) was smooth and had a uniform structure without any visible impurities, cracks, or agglomeration. With the addition of nanocellulose, the structuring of the surface (Figure 6b–6d) was observed when compared to neat nylon. This surface structuring could be due to the reorientation of hydrogen bonds in nylon polymeric chains due to the formation of new hydrogen bonds between nylon and nanocellulose (as seen previously) [51]. In the FESEM of cryo-fractured cross-section images, the thickness of all the films was around 50 µm (Figure 6e–6h). At higher magnification (Figure 6i), minute pores were observed in the neat nylon film due to solvent evaporation during the casting process. A few nanocellulose clusters were visible (marked with arrows) in the nanocomposite film at a low concentration of nanocellulose (0.1 and 0.5 wt%) (Figure 6j–6k), showing a better dispersion of nanocellulose in the nylon matrix. As the concentration of nanocellulose was increased to 1 wt% in the films, the pores were not visible (Figure 6l). These pores were closed due to the hydrogen bonding between nanocellulose and nylon and nanocellulose as a filler material that filled the pores, thus forming a denser structure required for high-barrier packaging applications.

### 3.5. Atomic force microscopy

The AFM micrograph of nanocellulose extracted from viscose-rayon yarn waste after 30 min of the hydrolysis reaction was performed on a 2×2 µm$^2$ sample size. It was observed that nanoparticles of irregular shape were present (Figure 7) and had an average diameter size of 65.03±10.15 nm. As previously reported in the literature, due to the many hydroxyl groups and high surface area [1, 54, 55], the drying process leads to agglomeration of nanocellulose during the AFM analysis, hence diminishing the specific surfaces by forming strong hydrogen bonds [56]. The TEM has seen similar fragmented forms in the literature [57].

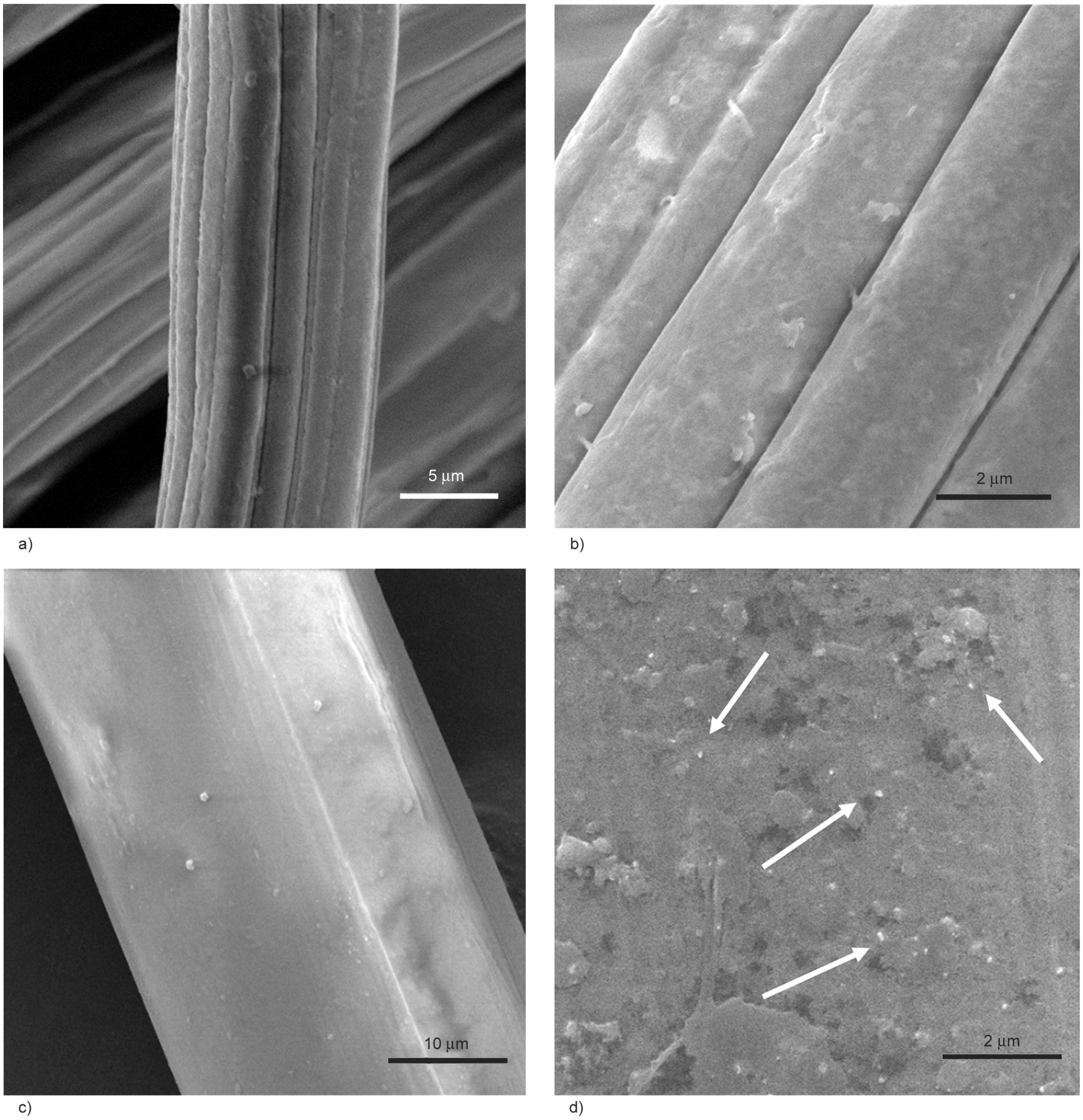

**Figure 4.** FESEM image of (a) viscose-rayon yarn waste, (b) viscose-rayon yarn waste magnified, (c) nylon yarn waste, and (d) nylon yarn waste magnified.

### 3.6. Differential scanning calorimetry

The crystallization behavior of nylon yarn waste and nylon films was investigated by DSC with first cooling and second heating curves, as shown in Figure 8. For nylon yarn waste, $T_m$ close to 219 °C signifies the presence of nylon-6 in the yarn waste [51]. The higher $T_{mc}$ of nylon yarn waste (186 °C) than the pure nylon-6 (180 °C) [58] might be attributed to the presence of nucleating agents in the yarn like talc powder, boron nitride, or any organic phosphates (as seen previously). From Figure 8a, fully developed melt crystallization peaks ($T_{mc}$) were observed for different samples during the cooling cycle. Clearly, the crystallization of nylon yarn occurred in a broad temperature range ($T_{onset}$ = 193.75 °C, $T_{endset}$ = 176.17 °C), whereas the crystallization of neat nylon and other films occurred in a narrow temperature regime ($T_{onset}$ = 191.94–193.38 °C, $T_{endset}$ = 178.5–177.16 °C), which signifies the effect of solvent processing favoring the crystallization of nylon by providing more mobility to the polymeric chains. A similar observation reported the effect of solvent processing on crystallization [36].

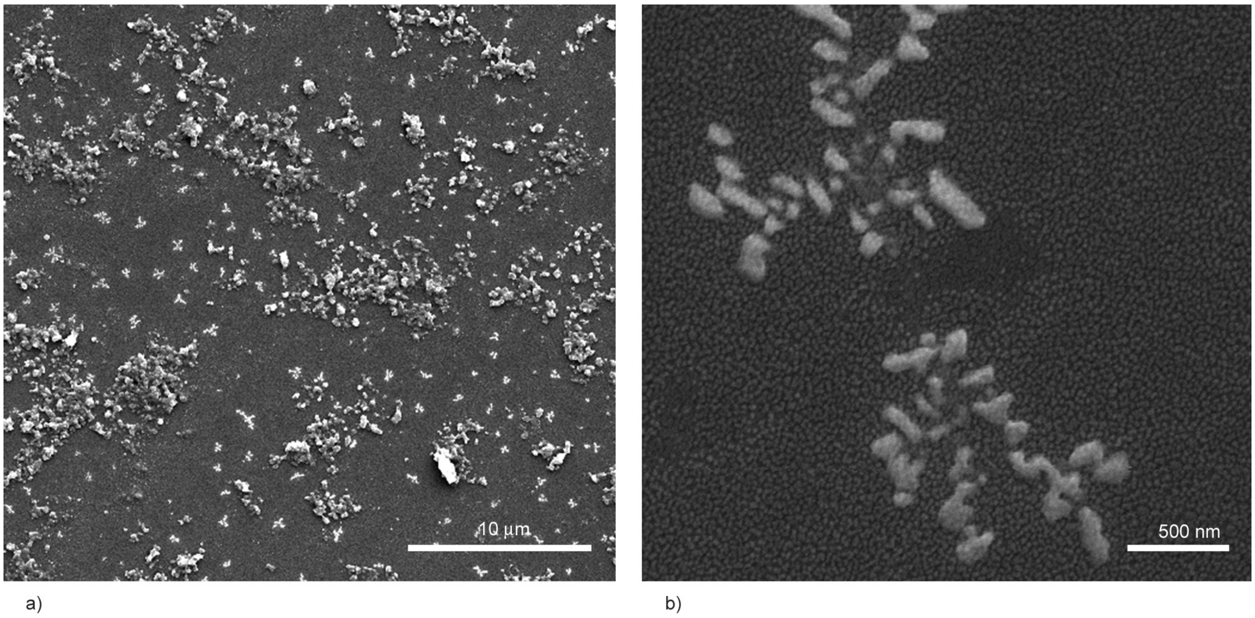

**Figure 5.** FESEM image of (a) nanocellulose and (b) magnified image of nanocellulose.

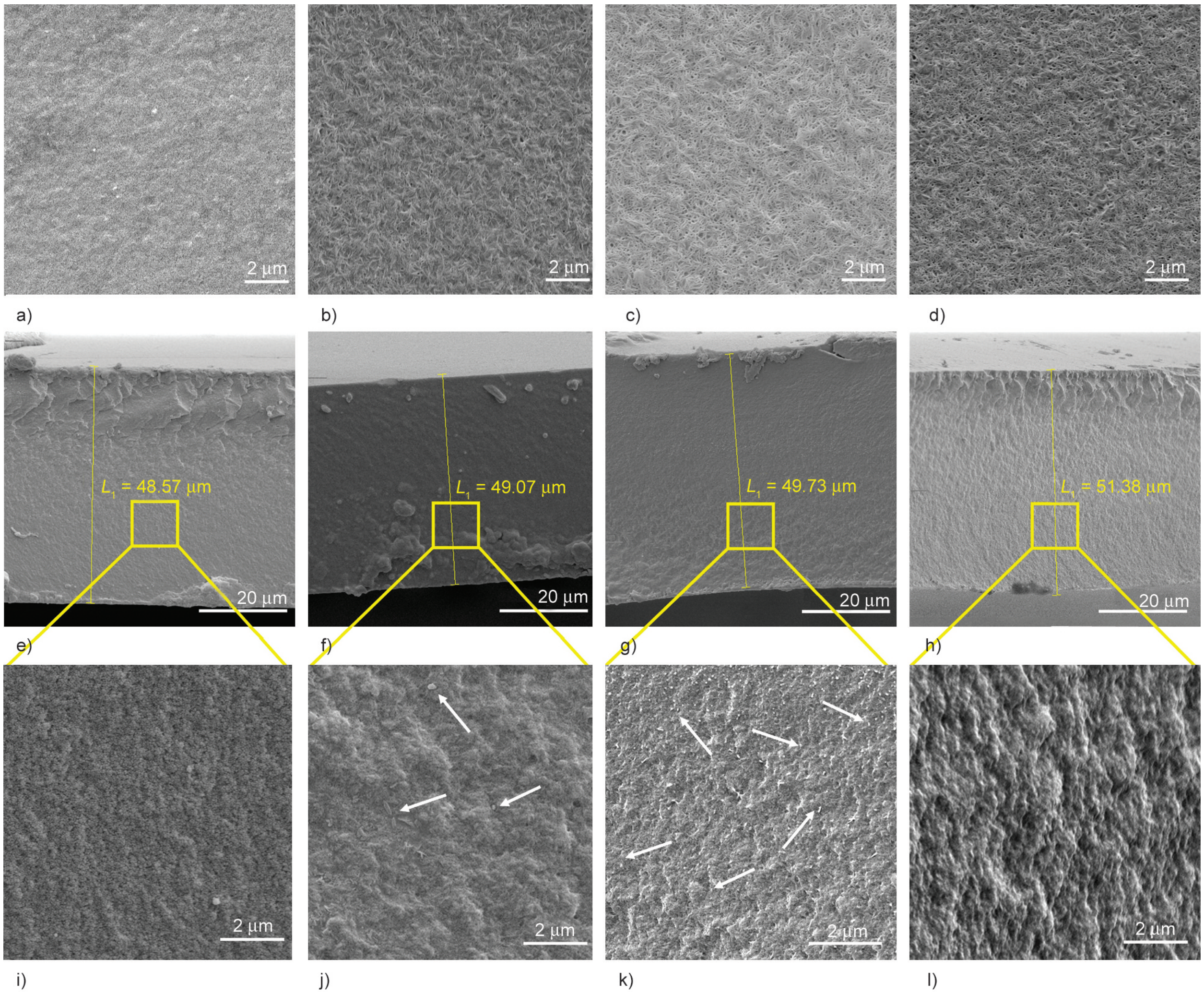

**Figure 6.** FESEM images of nylon- nanocellulose composite films illustrating the surface morphology of (a) neat nylon film, (b) Nylon-0.1% film, (c) Nylon-0.5% film, (d) Nylon-1% and cross-section morphology of (e) neat nylon film, (f) Nylon-0.1% film, (g) Nylon-0.5% film, (h) Nylon-1% film, and magnified cross-section of (i) neat nylon film, (j) Nylon-0.1% film, (k) Nylon-0.5% film, (l) Nylon-1% film.

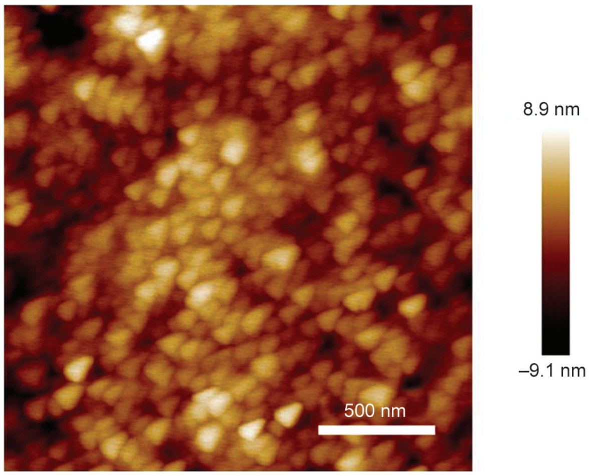

**Figure 7.** AFM image of nanocellulose extracted from viscose-rayon yarn waste.

Figure 8b reflects the glass transition temperature and melting peaks of nylon yarn and nylon nanocomposite films. Two melting peaks were observed, indicating γ-crystalline form and α-crystalline form, which were in line with previous DSC studies of nylon yarns [59]. Various thermal characteristics are summarized in Table 2. With the increasing concentrations of nanocellulose in nylon films, a slight decrease in $T_{mc}$ was observed, whereas the $T_g$ of films increased. Consequently, the crystallinity of films was also decreased with the increasing nanocellulose. Similar observations were reported when CNFs were incorporated into the nylon-6 matrix [51]. These effects are attributed to the strong interactions between hydroxyl groups of nanocellulose and the polar amide groups of nylon, which restricted the movement of nylon polymeric chains due to increased hydrogen bonding [51, 60] (seen previously from FTIR).

### 3.7. Thermogravimetric analysis

Figure 9 shows the weight loss curve of nylon yarn waste, neat nylon film, and nylon nanocomposite film (Nylon-1%). A 5 wt% residue was obtained for nylon yarn waste at 600 °C, confirming the presence of inorganic substances like talc in the nylon yarn (mentioned previously). In contrast, the residues for neat nylon film and Nylon-1% film were less than 1.5 wt%, confirming the removal of talc from the yarn's surface during the washing of the fibers. Some fluctuations were also visualized in the temperature range of 150–200 °C for nylon waste (marked with

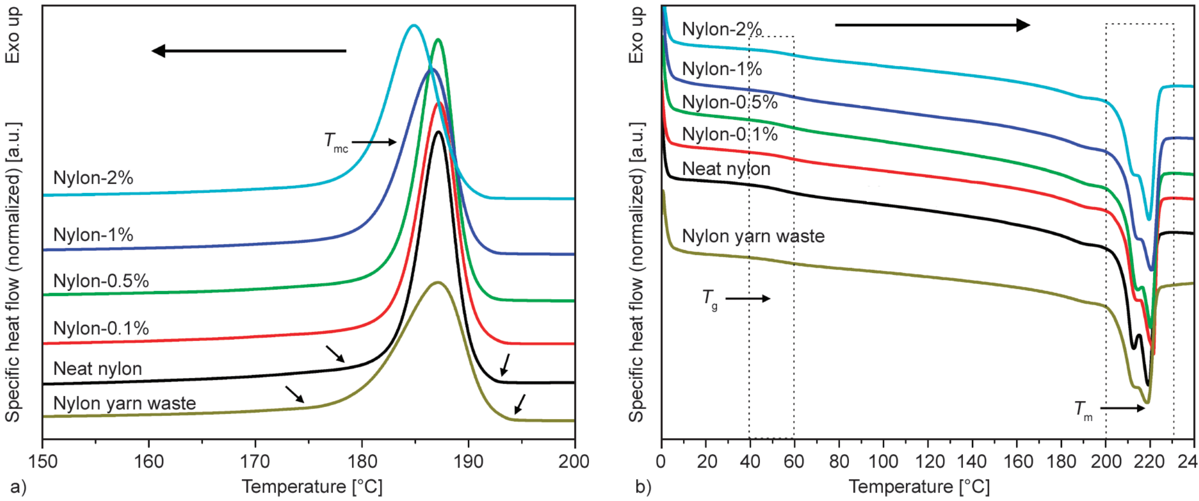

**Figure 8.** DSC curves of nylon yarn and nylon films during (a) first cooling and (b) second heating.

**Table 2.** DSC analysis for nylon yarn and nylon nanocomposite films.

| Sample | $T_{mc}$ [°C] | $T_g$ [°C] | $T_m$ [°C] | $\Delta H_m$ [J/g] | $X_c$ [%] |
|---|---|---|---|---|---|
| Nylon yarn waste | 186.17±0.76$^{b}$ | 54.00±0.30$^{a}$ | 219.50±0.50$^{b}$ | 60.17±0.76$^{d}$ | 31.67±0.38$^{c}$ |
| Neat nylon | 187.54±0.13$^{c}$ | 53.68±0.25$^{a}$ | 222.19±0.18$^{d}$ | 62.33±0.72$^{e}$ | 32.80±0.24$^{d}$ |
| Nylon-0.1% | 187.47±0.13$^{c}$ | 54.70±0.31$^{a,b}$ | 221.49±0.25$^{d}$ | 59.73±0.45$^{c,d}$ | 31.47±0.21$^{b,c}$ |
| Nylon-0.5% | 187.13±0.12$^{b,c}$ | 55.73±0.14$^{b,c}$ | 220.36±0.14$^{c}$ | 58.39±0.43$^{c}$ | 30.78±0.35$^{b}$ |
| Nylon-1% | 186.71±0.52$^{b,c}$ | 56.48±0.11$^{c,d}$ | 219.77±0.18$^{b,c}$ | 55.32±0.66$^{b}$ | 29.41±0.23$^{a}$ |
| Nylon-2% | 185.08±0.22$^{a}$ | 57.39±0.16$^{d}$ | 218.76±0.13$^{a}$ | 53.39±0.43$^{a}$ | 28.68±0.40$^{a}$ |

The mean and standard deviation are used to express the data.
$^{a,b,c,d}$Different letters in the same column indicate significant differences ($p < 0.05$).

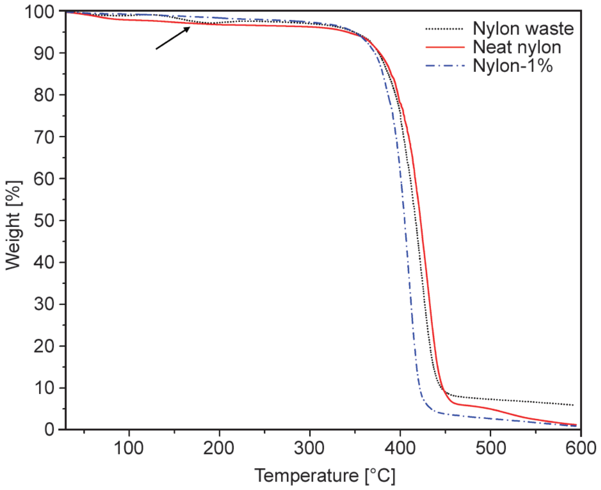

**Figure 9.** TGA curve for nylon yarn waste and nylon films.

arrow), which might be due to the release of some plasticizers from the nylon yarn. The film with nanocellulose showed an early degradation compared to neat nylon, which might be due to less thermal stability of cellulose when compared to nylon-6 [51]. In addition, a higher concentration of nanocellulose (1 wt%) might lead to an increased reorientation of hydrogen bonds, which result in the conversion of a fraction of α-crystalline form (stable) to γ-crystalline form (metastable) and consequently became less thermally stable.

## 3.8. Thickness and mechanical properties of films

The effect of nanocellulose on the film's mechanical properties, like tensile strength and elongation at break, was determined and presented in Table 2. With the addition of nanocellulose in the nylon films (up to 0.5 wt%), tensile strength decreased compared to neat film. However, the tensile strength remained similar to neat film at a maximum concentration of nanocellulose (1 wt%). The decrease in tensile strength (at low filler content) might be attributed to a few aggregates of nanocellulose in the nylon matrix, which were unable to disperse in the matrix due to the lower shear generated in response to the lower viscosity of the suspension. Although nanocellulose powder was freeze-dried to avoid the formation of aggregates and produce a porous, weakly bonded material [61], a few agglomerates might still be present in the powder. A similar case was observed where large agglomerates of microcrystalline cellulose (MCC) in PLA (polylactic acid) reduced the tensile strength of the composite [62]. Whereas, at higher filler concentration (1 wt%), higher suspension viscosity was achieved, leading to higher shear required to break the nanocellulose aggregates and disperse them uniformly in the matrix. In addition, for Nylon-1% film, the higher hydrogen bonding between cellulose and nylon, as observed from FTIR, might also be the reason for maintaining the higher tensile strength, similar to neat film. When comparing modulus (stiffness), the modulus decreased with the addition of nanocellulose when the concentration was 0.1 and 0.5 wt%. A decrease in stiffness of about 30.78% was observed, however, the modulus increased drastically to 1121 MPa when the concentration of nanocellulose was 1 wt% in nylon-6 matrix. This high modulus was in-line with the tensile strength observed at 1 wt% of nanocellulose. It can be seen that by adding a small amount of nanocellulose, the film's elasticity increased, and the strength and stiffness decreased, showing ductile behavior. However, at high nanocellulose content (1 wt%), the elongation, tensile, and modulus were like that of the neat nylon film. Although, it should be noted that the differences in tensile strength, elongation at break, and modulus for films were insignificant when considering standard deviation (Table 3).

**Table 3.** Mechanical properties of neat and nanocomposite films.

| Sample | Tensile strength [MPa] | Elongation at break [%] | Modulus [MPa] |
|---|---|---|---|
| Neat nylon | 20.43±2.03$^{a}$ | 10.81±5.45$^{a}$ | 1411±34$^{a}$ |
| Nylon-0.1% | 13.79±4.43$^{a}$ | 17.93±5.70$^{a}$ | 1040±25$^{a}$ |
| Nylon-0.5% | 13.95±1.67$^{a}$ | 11.81±2.13$^{a}$ | 976±128$^{a}$ |
| Nylon-1% | 19.05±1.89$^{a}$ | 10.82±1.09$^{a}$ | 1121±151$^{a}$ |

The mean and standard deviation are used to express the data. $^{a}$Different letters in the same column indicate significant differences ($p < 0.05$). (There are no significant diffences.)

## 3.9. Barrier properties: water contact angle and water vapor transmission rate of films

The water contact angles of the films were determined and presented in Figure 10. The contact angle decreased from 60.38° to 48.38° with the addition of nanocellulose. The nanocellulose being hydrophilic [63] has increased the surface wettability of the nylon films. One more reason for the decrease in contact angle could be the reorientation of the hydrogen bond at the surface of the nanocomposite films, as previously discussed in FTIR; and hydrogen bonding being highly polar [64] can have a lower contact angle

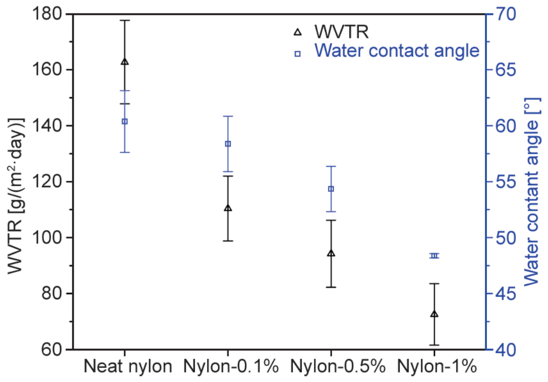

**Figure 10.** Water contact angle and WVTR of nanocomposite films.

with the water; hence the affinity of films towards water also increased.

The WVTR of the nylon films incorporated nanocelluloses were determined and presented in Figure 10. WVTR of the nanocomposite films significantly decreased compared to neat film. WVTR was decreased from 162.72 for neat films to 72.54 g/($m^2$·day) for Nylon-1% films. Similar results were achieved when nanoclay was added to the nylon matrix [58]. The decrease in WVTR of films is attributed to the increased surface structuring and dense cross-section of films (from FESEM images), leading to higher tortuosity for water vapors. The tortuous path created for moisture transfer by nanocellulose inside the nylon polymer matrix delays the transfer rate of water vapors. A similar observation was observed when CNC was incorporated in PLA [65] and PHB (polyhydroxybutyrate) [66] films. The nanocomposite film from textile yarn waste might create a new opportunity for application in packaging where a high barrier is required. Nevertheless, due to the water-sensitive nature of nylon-6 [18], the nanocomposite films should be sandwiched between the layers of water-insensitive polyolefins (PP or PE) for preparing multi-layered packaging [18] in order to take complete advantage of the engineered properties of developed films.

## 4. Conclusions

A high-water vapor barrier nylon nanocomposite films were successfully prepared using the solvent casting method utilizing acetic acid as a green solvent. Nanocellulose powder as a green nanofiller was extracted from the viscose-rayon textile yarn waste by acid hydrolysis and later introduced into the nylon matrix obtained from nylon textile yarn waste. Nanocellulose strongly interacted with the nylon matrix by forming new hydrogen bonds. In addition, nanocellulose also reoriented a few existing hydrogen bonds of nylon, as determined through FTIR and DSC. Consequently, nanocomposite films appeared dense with structuring at the surface (from FESEM), which increased the tortuosity for water vapors, and hence a maximum of 55% reduction in WVTR was noted for nylon films containing 1 wt% nanocellulose. However, the surface wettability of films was increased with the incorporation of nanocellulose. The tensile strength and elongation at break of nanocomposite films were changed with the addition of nanocellulose. The tensile strength decreased by 32.5%, elongation at break increased by 65.86%, and modulus decreased by 30.78% when 0.1 wt% of nanocellulose was added. However, at higher concentrations (1 wt%), the mechanical properties were similar to that of neat nylon films. The raw material analysis of nylon textile waste revealed the presence of around 5 wt% inorganic matter (TGA) that acted as a nucleating agent for nylon matrix (DSC). Nanocellulose did not act as a nucleating agent for the nylon matrix; rather, the crystallinity of nylon films decreased with the introduction of nanocellulose (DSC). The presence of plasticizers and antioxidants in nylon textile yarn waste was also evident from FTIR. Nevertheless, with nearly the same thermal properties as industrial-grade nylon-6, the pre-consumer nylon textile yarn waste could be a cheap alternative to expensive nylon-6 for various applications. Finally, the developed high-barrier nylon nanocomposite films may find an application where a low WVTR is required for packaging. More rigorous studies on the barrier properties of multi-layered packaging materials incorporating the developed nanocomposite film as a sandwich layer will be conducted in our future research.

## Acknowledgements

Prince Kumar Mishra would like to thank the Ministry of Education (MoE), Government of India, for providing resources and financial support to carry out this research work during his Master's study.

## References

[1] Wang Z., Yao Z., Zhou J., Zhang Y.: Reuse of waste cotton cloth for the extraction of cellulose nanocrystals. Carbohydrate Polymers, **157**, 945–952 (2017). https://doi.org/10.1016/j.carbpol.2016.10.044

[2] Mishra P. K., Izrayeel A. M. D., Mahur B. K., Ahuja A., Rastogi V. K.: A comprehensive review on textile waste valorization techniques and their applications. Environmental Science and Pollution Research, **29**, 65962–65977 (2022).
https://doi.org/10.1007/s11356-022-22222-6

[3] Ozger O. B., Girardi F., Giannuzzi G. M., Salomoni V. A., Majorana C. E., Fambri L., Baldassino N., Di Maggio R.: Effect of nylon fibres on mechanical and thermal properties of hardened concrete for energy storage systems. Materials and Design, **51**, 989–997 (2013).
https://doi.org/10.1016/j.matdes.2013.04.085

[4] Echeverria C. A., Handoko W., Pahlevani F., Sahajwalla V.: Cascading use of textile waste for the advancement of fibre reinforced composites for building applications. Journal of Cleaner Production, **208**, 1524–1536 (2019).
https://doi.org/10.1016/j.jclepro.2018.10.227

[5] Zhong X., Li R., Wang Z., Wang Y., Wang W., Yu D.: Highly flexible, transparent film prepared by upcycle of wasted jute fabrics with functional properties. Process Safety and Environmental Protection, **146**, 718–725 (2021).
https://doi.org/10.1016/j.psep.2020.12.013

[6] Aishwariya S.: Waste management technologies in textile industry. Innovative Energy and Research, **7**, 211 (2018).
https://doi.org/10.4172/2576-1463.1000211

[7] To M. H., Uisan K., Ok Y. S., Pleissner D., Lin C. S. K.: Recent trends in green and sustainable chemistry: Rethinking textile waste in a circular economy. Current Opinion in Green and Sustainable Chemistry, **20**, 1–10 (2019).
https://doi.org/10.1016/J.COGSC.2019.06.002

[8] Haslinger S., Ye Y., Rissanen M., Hummel M., Sixta H.: Cellulose fibers for high-performance textiles functionalized with incorporated gold and silver nanoparticles. ACS Sustainable Chemistry and Engineering, **8**, 649–658 (2020).
https://doi.org/10.1021/acssuschemeng.9b06385

[9] Colom X., Carrillo F.: Crystallinity changes in lyocell and viscose-type fibres by caustic treatment. European Polymer Journal, **38**, 2225–2230 (2002).
https://doi.org/10.1016/S0014-3057(02)00132-5

[10] Zeng H., Tang R-C.: Adsorption properties of direct dyes on viscose/chitin bicomponent fiber: Evaluation and comparison with viscose fiber. RSC Advances, **4**, 38064–38072 (2014).
https://doi.org/10.1039/C4RA05874G

[11] Chen H-L., Burns L. D.: Environmental analysis of textile products. Clothing and Textiles Research Journal, **24**, 248–261 (2006).
https://doi.org/10.1177/0887302X06293065

[12] Babu B. R., Parande A. K., Raghu S., Kumar T. P.: Cotton textile processing: Waste generation and effluent treatment. The Journal of Cotton Science, **11**, 141–153 (2007).

[13] Wang Y.: Fiber and textile waste utilization. Waste and Biomass Valorization, **1**, 135–143 (2010).
https://doi.org/10.1007/s12649-009-9005-y

[14] Stanescu M. D.: State of the art of post-consumer textile waste upcycling to reach the zero waste milestone. Environmental Science and Pollution Research, **28**, 14253–14270 (2021).
https://doi.org/10.1007/s11356-021-12416-9

[15] Montava-Jordà S., Torres-Giner S., Ferrandiz-Bou S., Quiles-Carrillo L., Montanes N.: Development of sustainable and cost-competitive injection-molded pieces of partially bio-based polyethylene terephthalate through the valorization of cotton textile waste. International Journal of Molecular Sciences, **20**, 1378 (2019).
https://doi.org/10.3390/ijms20061378

[16] Prado K. S., Gonzales D., Spinacé M. A. S.: Recycling of viscose yarn waste through one-step extraction of nanocellulose. International Journal of Biological Macromolecules, **136**, 729–737 (2019).
https://doi.org/10.1016/j.ijbiomac.2019.06.124

[17] Hufenus R., Yan Y., Dauner M., Kikutani T.: Melt-spun fibers for textile applications. Materials, **13**, 4298 (2020).
https://doi.org/10.3390/ma13194298

[18] Ammala A.: Nylon-MXD6 resins for food packaging. in ‘Multifunctional and nanoreinforced polymers for food packaging’ (ed.: Lagarón J-M.) Elsevier, Cambridge, Vol. 1, 243–260 (2011).
https://doi.org/10.1533/9780857092786.1.243

[19] Alonso-Montemayor F. J., Tarrés Q., Oliver-Ortega H., Espinach F. X., Narro-Céspedes R. I., Castañeda-Facio A. O., Delgado-Aguilar M.: Enhancing the mechanical performance of bleached hemp fibers reinforced polyamide 6 composites: A competitive alternative to commodity composites. Polymers, **12**, 1041 (2020).
https://doi.org/10.3390/polym12051041

[20] Shakiba M., Ghomi R. E., Khosravi F., Jouybar S., Bigham A., Zare M., Abdouss M., Moaref R., Ramakrishna S.: Nylon – A material introduction and overview for biomedical applications. Polymers for Advanced Technologies, **32**, 3368–3383 (2021).
https://doi.org/10.1002/pat.5372

[21] Dissanayake D. G. K., Weerasinghe D. U., Wijesinghe K. A. P., Kalpage K. M. D. M. P.: Developing a compression moulded thermal insulation panel using postindustrial textile waste. Waste Management, **79**, 356–361 (2018).
https://doi.org/10.1016/j.wasman.2018.08.001

[22] Šišková A. O., Pleva P., Hrůza J., Frajová J., Sedlaříková J., Peer P., Kleinová A., Janalíková M.: Reuse of textile waste to production of the fibrous antibacterial membrane with filtration potential. Nanomaterials, **12**, 50 (2021).
https://doi.org/10.3390/nano12010050

[23] Lee S., Jung S., Lin K-Y. A., Tsang Y. F., Kwon E. E.: Use of $CO_2$ and nylon as the raw materials for flammable gas production through a catalytic thermo-chemical process. Green Chemistry, **23**, 8922–8931 (2021).
https://doi.org/10.1039/D1GC02540F

[24] Cai Y., Li Q., Wei Q., Wu Y., Song L., Hu Y.: Structures, thermal stability, and crystalline properties of polyamide 6/organic-modified Fe-montmorillonite composite nanofibers by electrospinning. Journal of Materials Science, **43**, 6132–6138 (2008).
https://doi.org/10.1007/s10853-008-2921-6

[25] Bauer A. S., Tacker M., Uysal-Unalan I., Cruz R. M. S., Varzakas T., Krauter V.: Recyclability and redesign challenges in multilayer flexible food packaging – A review. Foods, **2021**, 2702 (2021). https://doi.org/10.3390/FOODS10112702

[26] Kiziltas A., Nazari B., Gardner D. J., Bousfield D. W.: Polyamide 6-cellulose composites: Effect of cellulose composition on melt rheology and crystallization behavior. Polymer Engineering and Science, **54**, 739–746 (2014). https://doi.org/10.1002/pen.23603

[27] Rahimi S. K., Otaigbe J. U.: The role of particle surface functionality and microstructure development in isothermal and non-isothermal crystallization behavior of polyamide 6/cellulose nanocrystals nanocomposites. Polymer, **107**, 316–331 (2016). https://doi.org/10.1016/j.polymer.2016.11.023

[28] Korkees F., Aldrees A., Barsoum I., Alshammari D.: Functionalised graphene effect on the mechanical and thermal properties of recycled PA6/PA6,6 blends. Journal of Composite Materials, **55**, 2211–2224 (2021). https://doi.org/10.1177/0021998320987897

[29] Janchai K., Boonmahitthisud A., Chaiwutthinan P., Chuayjuljit S., Hongrattanavichit I.: Property improvement of recycled nylon 6 by thermoplastic poly(etherester) elastomer and wollastonite. Materials Science Forum, **1053**, 47–51 (2022). https://doi.org/10.4028/p-ns1103

[30] Agarwal A., Raheja A., Natarajan T. S., Chandra T. S.: Effect of electrospun montmorillonite-nylon 6 nanofibrous membrane coated packaging on potato chips and bread. Innovative Food Science and Emerging Technologies, **26**, 424–430 (2014). https://doi.org/10.1016/J.IFSET.2014.09.012

[31] Purkayastha S., Dutta A., Ghosh A. K., Saha N. C.: Processability and performance property correlation for LDPE/PA6-based nanocomposite and its monolayer blown film for packaging application. Bulletin of Materials Science, **45**, 47 (2022). https://doi.org/10.1007/s12034-021-02627-8

[32] Paliwal R.: From waste to wealth: Stepping toward sustainability through circular economy. in 'Handbook of solid waste management' (eds.: Baskar C., Ramakrishna S., Baskar S., Sharma R., Chinnappan A., Sehrawat R.) Springer, Singapore, Vol. 1, 441–463 (2021).

[33] Tanwar R., Gupta V., Kumar P., Kumar A., Singh S., Gaikwad K. K.: Development and characterization of PVA-starch incorporated with coconut shell extract and sepiolite clay as an antioxidant film for active food packaging applications. International Journal of Biological Macromolecules, **185**, 451–461 (2021). https://doi.org/10.1016/j.ijbiomac.2021.06.179

[34] Mahmood S., Mandal U. K., Chatterjee B., Taher M.: Advanced characterizations of nanoparticles for drug delivery: Investigating their properties through the techniques used in their evaluations. Nanotechnology Reviews, **6**, 355–372 (2017). https://doi.org/10.1515/ntrev-2016-0050

[35] Liu K., Li Y., Tao L., Xiao R.: Preparation and characterization of polyamide 6 fibre based on a phosphorus-containing flame retardant. RSC Advances, **8**, 9261–9271 (2018). https://doi.org/10.1039/C7RA13228J

[36] Rastogi V. K., Samyn P.: Novel processing of polyhydroxybutyrate with micro- to nanofibrillated cellulose and effect of fiber morphology on crystallization behaviour of composites. Express Polymer Letters, **14**, 115–133 (2020). https://doi.org/10.3144/expresspolymlett.2020.11

[37] Li Y., Li G., Zou Y., Zhou Q., Lian X.: Preparation and characterization of cellulose nanofibers from partly mercerized cotton by mixed acid hydrolysis. Cellulose, **21**, 301–309 (2014). https://doi.org/10.1007/s10570-013-0146-6

[38] Alemdar A., Sain M.: Isolation and characterization of nanofibers from agricultural residues – Wheat straw and soy hulls. Bioresource Technology, **99**, 1664–1671 (2008). https://doi.org/10.1016/j.biortech.2007.04.029

[39] Carrillo F., Colom X., Suñol J., Saurina J.: Structural FTIR analysis and thermal characterisation of lyocell and viscose-type fibres. European Polymer Journal, **40**, 2229–2234 (2004). https://doi.org/10.1016/j.eurpolymj.2004.05.003

[40] Nelson M. L., O'Connor R. T.: Relation of certain infrared bands to cellulose crystallinity and crystal latticed type. Part I. Spectra of lattice types I, II, III and of amorphous cellulose. Journal of Applied Polymer Science, **8**, 1311–1324 (1964). https://doi.org/10.1002/APP.1964.070080322

[41] Rizal S., Olaiya F. G., Saharudin N. I., Abdullah C. K., Olaiya N. G., Haafiz M. K., M., Yahya E. B., Sabaruddin F. A., Ikramullah, Khalil H. P. S. A.: Isolation of textile waste cellulose nanofibrillated fibre reinforced in polylactic acid-chitin biodegradable composite for green packaging application. Polymers, **13**, 325 (2021). https://doi.org/10.3390/polym13030325

[42] Oh S. Y., Yoo D. I., Shin Y., Kim H. C., Kim H. Y., Chung Y. S., Park W. H., Youk J. H.: Crystalline structure analysis of cellulose treated with sodium hydroxide and carbon dioxide by means of X-ray diffraction and FTIR spectroscopy. Carbohydrate Research, **340**, 2376–2391 (2005). https://doi.org/10.1016/j.carres.2005.08.007

[43] Popescu C-M., Singurel G., Popescu M-C., Vasile C., Argyropoulos D. S., Willför S.: Vibrational spectroscopy and X-ray diffraction methods to establish the differences between hardwood and softwood. Carbohydrate Polymers, **77**, 851–857 (2009). https://doi.org/10.1016/j.carbpol.2009.03.011

[44] Tegginamata P., Ravindrachary V., Mahantesha B. K., Sahanakumari R., Ramani R., Kotresh T. M., Ananth S.: CdO nano-particles induced structural, thermal, surface morphological and electrical properties of Nylon-6. in 'AIP Conference Proceedings. Manglore, India' Vol. 2244, 070022 (2020). https://doi.org/10.1063/5.0009367

[45] Yu X., Jiang Y., Wu Q., Wei Z., Lin X., Chen Y.: Preparation and characterization of cellulose nanocrystal extraction from pennisetum hydridum fertilized by municipal sewage sludge *via* sulfuric acid hydrolysis. Frontiers in Energy Research, **9**, 653 (2021).
https://doi.org/10.3389/fenrg.2021.774783

[46] Kusmono, Listyanda R. F., Wildan M. W., Ilman M. N.: Preparation and characterization of cellulose nanocrystal extracted from ramie fibers by sulfuric acid hydrolysis. Heliyon, **6**, e05486 (2020).
https://doi.org/10.1016/j.heliyon.2020.e05486

[47] Segal L., Creely J. J., Martin A. E., Conrad C. M.: An empirical method for estimating the degree of crystallinity of native cellulose using the X-ray diffractometer. Textile Research Journal, **29**, 786–794 (1959).
https://doi.org/10.1177/004051755902901003

[48] Kruer-Zerhusen N., Cantero-Tubilla B., Wilson D. B.: Characterization of cellulose crystallinity after enzymatic treatment using fourier transform infrared spectroscopy (FTIR). Cellulose, **25**, 37–48 (2018).
https://doi.org/10.1007/s10570-017-1542-0

[49] Giller C. B., Chase D. B., Rabolt J. F., Snively C. M.: Effect of solvent evaporation rate on the crystalline state of electrospun nylon 6. Polymer, **51**, 4225–4230 (2010).
https://doi.org/10.1016/j.polymer.2010.06.057

[50] Sallem-Idrissi N., Sclavons M., Debecker D. P., Devaux J.: Miscible raw lignin/nylon 6 blends: Thermal and mechanical performances. Journal of Applied Polymer Science, **133**, 42963 (2016).
https://doi.org/10.1002/app.42963

[51] Sridhara P. K., Masso F., Olsén P., Vilaseca F.: Strong polyamide-6 nanocomposites with cellulose nanofibers mediated by green solvent mixtures. Nanomaterials, **11**, 2127 (2021).
https://doi.org/10.3390/nano11082127

[52] Ossman M., Fatah M. A., Ossman M. E., Mansour M. S., Fattah M. A., Taha N., Kiros Y.: Peanut shells and talc powder for removal of hexavalent chromium from aqueous solutions. Bulgarian Chemical Communications, **46**, 629–639 (2014).

[53] Sharma P., Ahuja A., Dilsad Izrayeel A. M., Samyn P., Rastogi V. K.: Physicochemical and thermal characterization of poly(3-hydroxybutyrate-*co*-4-hydroxybutyrate) films incorporating thyme essential oil for active packaging of white bread. Food Control, **133**, 108688 (2022).
https://doi.org/10.1016/j.foodcont.2021.108688

[54] Yue Y., Zhou C., French A. D., Xia G., Han G., Wang Q., Wu Q.: Comparative properties of cellulose nanocrystals from native and mercerized cotton fibers. Cellulose, **19**, 1173–1187 (2012).
https://doi.org/10.1007/s10570-012-9714-4

[55] Xiong R., Zhang X., Tian D., Zhou Z., Lu C.: Comparing microcrystalline with spherical nanocrystalline cellulose from waste cotton fabrics. Cellulose, **19**, 1189–1198 (2012).
https://doi.org/10.1007/s10570-012-9730-4

[56] Lu P., Hsieh Y-L.: Cellulose isolation and core–shell nanostructures of cellulose nanocrystals from chardonnay grape skins. Carbohydrate Polymers, **87**, 2546–2553 (2012).
https://doi.org/10.1016/j.carbpol.2011.11.023

[57] Chen G-Y., Yu H-Y., Zhang C-H., Zhou Y., Yao J-M.: A universal route for the simultaneous extraction and functionalization of cellulose nanocrystals from industrial and agricultural celluloses. Journal of Nanoparticle Research, **18**, 48 (2016).
https://doi.org/10.1007/s11051-016-3355-8

[58] Allafi A. R., Pascall M. A.: The effect of different percent loadings of nanoparticles on the barrier and thermal properties of nylon 6 films. Innovative Food Science and Emerging Technologies, **20**, 276–280 (2013).
https://doi.org/10.1016/j.ifset.2013.08.009

[59] Klata E., van de Velde K., Krucińska I.: DSC investigations of polyamide 6 in hybrid GF/PA6 yarns and composites. Polymer Testing, **22**, 929–937 (2003).
https://doi.org/10.1016/S0142-9418(03)00043-6

[60] Sunday D. F., Green D. L.: Thermal and rheological behavior of polymer grafted nanoparticles. Macromolecules, **48**, 8651–8659 (2015).
https://doi.org/10.1021/acs.macromol.5b00987

[61] Dufresne A.: Cellulose nanomaterials as green nanoreinforcements for polymer nanocomposites. Philosophical Transactions of the Royal Society A: Mathematical, Physical and Engineering Sciences, **376**, 20170040 (2018).
https://doi.org/10.1098/rsta.2017.0040

[62] dos Santos F. A., Iulianelli G. C. V., Tavares M. I. B.: Effect of microcrystalline and nanocrystals cellulose fillers in materials based on PLA matrix. Polymer Testing, **61**, 280–288 (2017).
https://doi.org/10.1016/j.polymertesting.2017.05.028

[63] Seoane I. T., Cerrutti P., Vazquez A., Manfredi L. B., Cyras V. P.: Polyhydroxybutyrate-based nanocomposites with cellulose nanocrystals and bacterial cellulose. Journal of Polymers and the Environment, **25**, 586–598 (2017).
https://doi.org/10.1007/s10924-016-0838-8

[64] Yamabe S., Morokuma K.: Molecular orbital studies of hydrogen bonds. IX. Electron distribution analysis. Journal of the American Chemical Society, **97**, 4458–4465 (1975).
https://doi.org/10.1021/ja00849a003

[65] Fortunati E., Peltzer M., Armentano I., Torre L., Jiménez A., Kenny J. M.: Effects of modified cellulose nanocrystals on the barrier and migration properties of PLA nano-biocomposites. Carbohydrate Polymers, **90**, 948–956 (2012).
https://doi.org/10.1016/J.CARBPOL.2012.06.025

[66] Dhar P., Bhardwaj U., Kumar A., Katiyar V.: Poly(3-hydroxybutyrate)/cellulose nanocrystal films for food packaging applications: Barrier and migration studies. Polymer Engineering and Science, **55**, 2388–2395 (2015).
https://doi.org/10.1002/PEN.24127